Interwake Turbulence Properties of Homogeneous Dilute Particle-Laden Flows

J.-H. Chen[*] and G. M. Faeth[†]
University of Michigan, Ann Arbor, Michigan 48109-2140

The properties of turbulence generated by uniform fluxes of monodisperse spherical particles moving through a uniform flowing gas were studied experimentally, emphasizing the properties of the region surrounding individual wake disturbances, i.e., the turbulent interwake region. Mean and fluctuating values, probability density functions, and energy spectra of streamwise and cross-stream velocities were measured within a counterflowing particle/air wind tunnel using particle wake discriminating laser velocimetry. Test conditions included nearly monodisperse glass spheres having diameters of 0.5–2.2 mm, particle Reynolds numbers of 106–990, mean particle spacings of 13–208 mm, particle volume fractions less than 0.003%, direct rates of dissipation of turbulence by particles less than 4%, and turbulence generation rates sufficient to yield streamwise relative turbulence intensities in the range 0.2–1.5%. The turbulent interwake region was homogeneous and nearly isotropic with probability density functions that are well approximated by Gaussian functions. Relative turbulence intensities were correlated effectively based on an analogy to the properties of isotropic grid-generated turbulence by scaling with the mean particle spacing normalized by the particle wake momentum diameter. For present turbulence generation conditions the turbulent interwake region had turbulence Reynolds numbers of 0.4–3.5 and was in the final decay period where vortical regions fill the turbulent interwake region but are sparse. This implies enhanced rates of dissipation of turbulent kinetic energy and decreasing macroscale/microscale ratios of the turbulence with increasing Reynolds numbers, as opposed to increasing ratios with increasing Reynolds numbers typical of conventional fully developed isotropic turbulence.

Nomenclature

A	= dimensionless integral length scale; Eq. (10)
C_d	= particle drag coefficient
D	= dissipation factor; Eq. (7)
D_P	= Parthasarathy dissipation factor; Eq. (8)
d_p	= particle diameter
$E_u(k)$	= streamwise energy spectrum
f	= frequency
K	= kurtosis of probability density function (PDF)
k	= wave number, $2\pi/s$
L_u	= streamwise integral length scale
ℓ_K	= Kolmogorov length scale, $(\nu^3/\varepsilon)^{1/4}$
ℓ_p	= mean particle spacing; Eq. (1)
M	= mesh size of a grid
n	= power in turbulence decay law; Eq. (4)
n''	= particle number flux
Re	= particle Reynolds number, $d_p U_p / \nu$
Re_λ	= turbulence Reynolds number, $Re_\lambda = \lambda \bar{u}'/\nu$
S	= skewness of PDF
s	= distance
t_K	= Kolmogorov time scale, $(\nu/\varepsilon)^{1/2}$
U_p	= mean streamwise relative velocity of a particle
u	= streamwise gas velocity
u_K	= Kolmogorov velocity scale, $(\varepsilon\nu)^{1/4}$
v	= cross-stream gas velocity
x	= streamwise distance
x_o	= streamwise virtual origin location
β	= empirical factor; Eqs. (4) and (5)
ε	= rate of dissipation of turbulence kinetic energy
θ	= wake momentum diameter, $(C_d d_p^2/8)^{1/2}$
λ	= Taylor length scale; Eq. (3)
ν	= molecular kinematic viscosity of air

Superscripts

$(\bar{\ })$	= mean value
$(\bar{\ })'$	= rms fluctuating value
$(\bar{\ })'^2$	= mean-square fluctuating value

Introduction

TURBULENCE generation is the direct disturbance of the continuous-phase velocity field by the wakes of dispersed-phase objects in dispersed multiphase flows. Turbulence generation supplements the conventional production of turbulence caused by mean velocity gradients in the continuous phase. Turbulence generation is most important when the dispersed-phase objects have large relative velocities (large Reynolds numbers) and relatively large relaxation times compared to characteristic turbulence times. Such conditions are typical of many practical dispersed multiphase flows having significant separated-flow effects, e.g., sprays, particle-laden jets, bubbly jets, rainstorms, etc. In spite of its importance, however, turbulence generation has not received much attention so that current understanding and capabilities for predicting its properties are very limited. Motivated by these observations, the objective of the present investigation was to extend past studies of turbulence generation in this laboratory[1−3] to consider the properties of the continuous-phase region surrounding individual particle (drop) wake disturbances, i.e., the turbulent interwake region.

Earlier observations of flows resulting from turbulence generation in this laboratory have involved uniform fluxes of nearly monodisperse spherical particles moving at near terminal velocities in still water,[1] still air,[2] and upflowing air.[3] The resulting flows are homogeneous and stationary with turbulence production entirely caused by turbulence generation. An interesting feature of these flows is that the local rate of dissipation of turbulence kinetic energy mainly controls continuous-phase turbulence properties and that this parameter is readily found as the local rate of loss of particle mechanical energy per unit volume (the particle dissipation rate). All other continuous-phase properties of the flow [moments, probability density functions (PDFs), spectra, etc.], however, are not known and must be related to particle properties and particle dissipation rates.

The most recent study in this laboratory, involving particles in upflowing air,[3] avoided earlier problems of measurements in still environments that yielded flows having very large turbulence

intensities.[1,2] It was found that relative turbulence intensities were proportional to the square root of the rate of dissipation in accord with a simplified stochastic theory of turbulence generation described in Refs. 1 and 2. Other properties, however, were not explained by the simplified stochastic theory and exhibited features not seen in conventional homogeneous turbulence: PDFs of streamwise velocities were not Gaussian, whereas PDFs of cross-stream velocities were Gaussian, and the energy spectra of both velocity components exhibited prominent -1 power decay regions in addition to the usual $-\frac{5}{3}$ power decay inertial region. These differences from conventional turbulence properties were attributed to effects of particle wakes that cannot be separated from other flow properties by conventional phase-discriminating velocity measurements because the arrival of particle wakes in these flows is random. Detailed observations, however, showed that particle wake properties approximated the properties of the laminarlike turbulent wakes observed for particle wakes at intermediate Reynolds numbers in conventional turbulent environments, described in Refs. 4–6, in spite of the unusual features of continuous-phase turbulence resulting from turbulence generation. Given estimates of the wake properties, it was subsequently shown that most practical turbulence generation processes involve particle wake disturbances surrounded by a relatively large turbulent interwake region.[7]

Stochastic analysis to estimate the overall properties of flows dominated by turbulence generation involves straightforward conditional averaging of the properties of the wake disturbances and the turbulent interwake region. At the present time information is available concerning the laminarlike turbulent wake behavior of the wake disturbances[5,6] and the overall properties of flows dominated by turbulence generation.[1–3] The missing element for predictions of the overall flow properties of turbulence generation involves information about the properties of the turbulent interwake region. Thus, the objectives of the present investigation were to complete conditional measurements of the properties of the turbulent interwake region for the range of conditions considered in Ref. 3 and to exploit existing methods in the turbulence literature to interpret and correlate the measurements.

Present measurements were carried out in a counterflow particle/air wind tunnel considering nearly monodisperse glass spheres having particle fluxes sufficient to yield relative turbulence intensities of 0.2–1.5%. Measurements were made using particle wake discriminating laser velocimetry to find moments and PDFs of velocities, energy spectra of streamwise velocity fluctuations, and characteristic time and length scales. These results were interpreted and correlated by studying potential analogies between the turbulent interwake region of turbulence generation processes and homogeneous grid-generated turbulence, e.g., the studies of grid-generated turbulence of Refs. 8–12 and references cited therein. The present description of the study is brief; more details and a tabulation of the data can be found in Chen et al.[3]

Experimental Methods

The apparatus consisted of a vertical counterflow wind tunnel with upflowing air moving toward the suction side of the blower and freely falling nearly monodisperse spherical glass particles that were introduced at the top of the wind tunnel using a particle feeder (see Ref. 3 for a complete description). The air flowpath consisted of a rounded inlet, a flow straightener, and a 16:1 contraction ratio to the 305 × 305 mm cross-section windowed test section. The particle flowpath consisted of a variable-speed particle feeder, a screen array particle dispersion section, a honeycomb particle flow straightener, and a particle acceleration section to yield near terminal velocity particles at the test section. The particles were collected in a flexible plastic funnel below the air inlet.

Measurements included particle number fluxes by sampling and particle and gas velocities by a traversable laser velocimetry (LV) system. The particle measurements are described in Ref. 3; therefore, the following discussion will be limited to the gas velocity measurements. A single-channel, dual-beam, forward-scatter, frequency-shifted LV was used, based on the 514.5-nm line of an argon-ion laser. Streamwise and cross-stream velocities were found by rotating the optics accordingly. A beam expander was used to yield a measuring volume diameter and length of 55 and 425 μm,

respectively. The airflow entering the wind tunnel was seeded with oil drops having a 1-μm nominal diameter for the air velocity measurements. Velocities were found from the low-pass filtered analog output of a burst counter signal processor. The combination of frequency shifting plus a constant sampling rate of the analog output of the signal processor eliminated effects of directional bias and ambiguity and velocity bias. The glass particles were inspected with a microscope after they were collected, which showed that the particles did not collect seeding particles and were not damaged during passage through the test apparatus; therefore, they were reused. Heavy seeding levels were used so that effects of LV step noise were deferred to scales roughly an order of magnitude larger than the Kolmogorov scales. In spite of the heavy seeding, however, effects of turbulence modulation by LV seeding particles were small. For example, the seeding particles had good response for present test conditions so that effects of slip were small. For such conditions the locally homogeneous flow approximation is acceptable, and effects of turbulence modulation by seeding particles are reflected by the increased apparent density of the continuous phase caused by the presence of the seeding particles. With seeding particle volume fractions smaller than 2×10^{-7}, however, the density increase was less than 0.02% with correspondingly small effects of turbulence modulation.

Conditional sampling was carried out by installing a particle detector so that disturbances from particle wakes could be deleted from the velocity record. The particle detection system consisted of a He–Ne laser sheet whose width was controlled by an adjustable slot. The sheet was observed through a laser line filter from a direction nearly normal to the path of the sheet, using another adjustable slot to control the length of the sheet that was observed. The LV measuring volume was positioned just below the He–Ne laser sheet at the center of the region observed. The required dimensions of the region of the laser sheet that was observed were estimated according to the laminarlike turbulent wake correlations of Refs. 5 and 6. The region included had a radius larger than twice the characteristic laminarlike wake radius (as defined in Refs. 5 and 6) from the particle wake axis. When strong scattering from a glass sphere was detected, velocity signals were not processed to contribute to the conditional properties of the turbulent interwake region for the time required for the particle wake to pass through the measuring plane. This time was selected so that the maximum mean velocity defect of the wake disturbance at the plane of the measurements was smaller than the velocity fluctuation level of the turbulent interwake region. Saturation of the particle detector occasionally allowed wake disturbances from a nearby particle to be recorded; such conditions were treated using velocity amplitude discrimination as discussed in Ref. 3. Finally, PDFs of streamwise and cross-stream velocities were used to access the effectiveness of the particle wake discrimination system as discussed later.

Velocity records having drop-out periods that resulted when disturbances caused by particle wakes were removed were analyzed directly by correcting the sampling time for most velocity statistics, e.g., moments and other PDF properties. In contrast, obtaining correct temporal power spectra in the presence of dropout periods requires special treatment as described by Buchhave[13] and Buchhave et al.[14] (see Ref. 3 for the present application of these methods). Upflow velocities in the wind tunnel were set to provide absolute turbulence intensities less than 15% so that LV measuring conditions were excellent. Therefore, use of Taylor's hypothesis to convert measured temporal power spectra and scales to spatial spectra and scales is appropriate.[10] Sampling periods were adjusted to provide experimental uncertainties (95% confidence) less than 5% for mean velocities, less than 10% for rms velocity fluctuations, less than 10% for PDFs within one standard deviation of the most probable velocity and less than 20% for temporal power spectra at frequencies smaller than the reciprocal of the temporal integral scale with uncertainties smaller elsewhere.

Test conditions are summarized in Table 1. Particle properties were measured as described in Ref. 3. The particles were nearly monodisperse with standard deviations of particle diameters less than 10% of the mean particle diameters (Table 1). The particles approached terminal velocity conditions so that wake properties were quasisteady and the multiphase flow was approximately

Table 1 Summary of test conditions[a]

Parameter	Nominal particle diameter (mm)[b]		
	0.5 (0.047)	1.1 (0.109)	2.2 (0.126)
U_p, mm/s	3370	5530	7000
Re	106	373	990
C_d	1.22	0.79	0.54
$(dU_p/dx)/U_p$, %/m	2	11	14
θ, mm	0.183	0.299	0.519
n'', kpart/m²s	71–950	4–56	0.5–10
ℓ_p, mm	13–32	41–97	77–208
ε, m²/s³	0.088–1.17	0.041–0.54	0.012–2.3
ℓ_K, mm	0.2–0.5	0.3–0.6	0.4–0.7
t_K, ms	4–14	5–16	8–37
u_K, mm/s	34–60	31–54	21–44
$\bar{u}'/U_p$, %	0.5–1.5	0.2–0.6	0.2–0.6
λ, mm	0.7–0.9	0.6–0.8	1.2–1.8
Re_λ	0.7–2.5	0.4–1.5	1.4–3.5
L_u, mm	11–35	42–178	23–156

[a] Round glass beads (density of 2500 kg/m³) falling in upflowing air at standard temperature and pressure (air density of 1.16 kg/m³ and kinematic viscosity of 15.9 mm²/s) having a mean velocity of 1.1 m/s. Parameter ranges for each particle size given in order of lowest–highest particle number fluxes, respectively.
[b] Standard deviations given in parentheses.

homogeneous (e.g., rates of particle acceleration at the measuring location were in the range 2–14% of the mean particle velocity per meter); nevertheless, measured particle velocities at the measuring location were used to find other particle properties rather than assuming terminal velocity conditions. Assuming that the particles are falling randomly, the mean particle spacing is given by

$$\ell_p = [(U_p - \bar{u})/n'']^{\frac{1}{3}} \qquad (1)$$

which yields values of 13–208 mm with corresponding particle volume fractions less than 0.003%.

The direct dissipation of turbulence kinetic energy (dissipation) by particles was less than 4%; see Chen[7] for a discussion of this estimate. In addition, dissipation within the wake disturbances was also small compared to the turbulent interwake region. This can be seen by noting that dissipation from mean velocities in the wake disturbances is small because of the small Mach numbers of these flows so that the ratio of the dissipation in the interwake region to the flow as a whole can be estimated by the corresponding estimate of the ratio of the turbulence kinetic energies of these two regions. This latter ratio is best estimated by the ratio of the square of the cross-stream velocities of these two regions (to avoid bias of the overall fluctuations by mean velocities in the wake disturbances) yielding a value of 88% (Ref. 7). This implies that dissipation within the wake disturbances is only roughly 12% of the total dissipation, which is smaller than the experimental uncertainties of turbulence kinetic energies (mean square velocity fluctuations); therefore, a reasonable approximation for the rate of dissipation in the turbulent interwake region can be found from the rate of turbulence generation by the particles, as follows:

$$\varepsilon = \pi n'' d_p^2 C_d U_P^2 \big| \, 8 \qquad (2)$$

Given ε, the Kolmogorov scales can be computed from their definitions. For these dissipation rates relative turbulence intensities caused by turbulence generation were in the range 0.2–1.5%. Measurements to be discussed later will show that interwake turbulence is similar to homogeneous isotropic turbulence so that Taylor's dissipation length scale can be estimated from the following equation:

$$\lambda = (15\nu \bar{u}'^2/\varepsilon)^{\frac{1}{2}} \qquad (3)$$

Present values of λ are somewhat larger but comparable to Kolmogorov length scales (i.e., $\lambda/\ell_K = 1.3$–3.5), which is not unexpected in view of the relatively small turbulence Reynolds numbers 0.4–3.5 of the present turbulent interwake regions. Finally, streamwise integral length scales were obtained from energy spectra as discussed later, yielding values comparable to mean particle spacings, i.e., 11–178 mm.

Evaluation of the apparatus is discussed by Chen et al.[3] and Chen.[7] Measurements of particle number fluxes and phase velocities showed that they varied less than experimental uncertainties

over the central 205 × 205 mm cross section of the flow, extending 200 mm in the streamwise direction, which surrounded the location where measurements were made. Similar measurements showed that flow properties varied less than experimental uncertainties as a function of time. Thus, present flows were properly homogeneous and stationary with turbulence within the turbulent interwake region produced by turbulence generation.

Results and Discussion

Relative Turbulence Intensities

Correlations of the properties of the turbulent interwake region were sought by drawing analogies between the turbulent interwake region and grid-generated turbulence. Past experimental observations show that turbulence downstream of grids can be divided into three regions: 1) a developing region near the grids, where the wakes from grid elements are merging and the turbulent flow is inhomogeneous and anisotropic; 2) an initial-decay region where the turbulent flow is nearly homogeneous and is locally isotropic; and 3) a final-decay region, where viscous effects dominate, regions containing vorticity become sparse (giving the appearance of isolated turbulent spots from single-point measurements), and the turbulence decays more rapidly than in the initial decay region. Thus, comparing the turbulent interwake region with grid-generated turbulence suggests that the wake disturbances of turbulence generation correspond to the developing region of grid-generated turbulence and that the turbulent interwake region of turbulence generation corresponds to either the initial- or final-decay regions of grid-generated turbulence. Batchelor and Townsend[11,12] suggest a value of $Re_\lambda \approx 5$ as the condition for the onset of the final-decay region for grid-generated turbulence; therefore, the present turbulent interwake regions involving $Re_\lambda \approx 0.4$–3.5 (see Table 1) have significant potential for behavior analogous to the final decay region.

The analogy between the present turbulent interwake region and grid-generated turbulence was based on an expression for grid-generated turbulence from Batchelor and Townsend,[11,12] as follows:

$$(\bar{u}' \text{ or } \bar{v}')/\bar{u} = \beta[C_d M/(x - x_o)]^n \qquad (4)$$

where β is an empirical factor and they propose $n = \frac{1}{2}$ and $\frac{5}{4}$ in the initial- and final-decay periods, respectively. For present conditions the turbulent interwake region was homogeneous; therefore, a reasonable analogy to the distance from the grid for grid-generated turbulence is a distance on the order of the mean particle spacing. The length corresponding to the product of mesh size and drag coefficient for grid-generated turbulence was taken to be the particle wake momentum diameter θ, which similarly involves the product of the particle diameter and drag coefficient. Given these analogies, the expression corresponding to Eq. (4) for the turbulent interwake region becomes

$$(\bar{u}' \text{ or } \bar{v}')/U_p = \beta(\theta/\ell_p)^n \qquad (5)$$

where β may not necessarily be the same for $\bar{u}'$ and $\bar{v}'$. Introducing expressions for θ in terms of C_d and d_p, Eq. (1) for ℓ_p, and eliminating n'' from the resulting expression using Eq. (2) yields the following potential correlation for the relative turbulence intensities of the turbulent interwake region:

$$(\bar{u}' \text{ or } \bar{v}')/U_p = \beta D^{n/3} \qquad (6)$$

where D is a dimensionless dissipation factor defined as follows:

$$D = (\theta/\ell_p)^3 = \frac{\varepsilon d_p (C_d/8)^{\frac{1}{2}}}{\pi U_p^2 (U_p - \bar{u})} \qquad (7)$$

During the earlier turbulence generation studies of Refs. 1 and 2, expressions very similar to Eqs. (6) and (7) were developed that proved to be reasonably effective for correlating their relative turbulence intensity measurements. Their expression was developed using a simple stochastic analysis to synthesize the properties of particle wake disturbances alone (with no consideration of a turbulent interwake region) based on Campbell's theorem, similar to the analysis of electrical noise from Rice.[15] The resulting correlation was identical to Eq. (6) except that D was replaced by an alternative dimensionless dissipation factor D_P, defined as follows:

$$D_P = \varepsilon d_p (C_d/8)^{\frac{1}{3}} \big| \, U_p^3 \qquad (8)$$
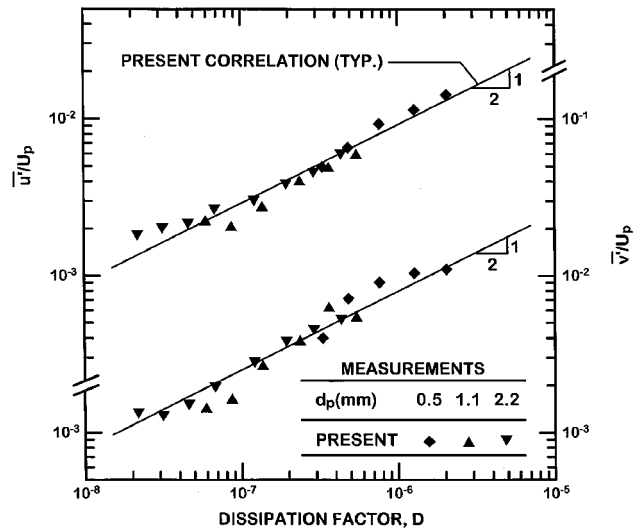
Fig. 1 Streamwise and cross-stream relative turbulence intensities as a function of the dissipation factor for various particle sizes.

The dimensionless dissipation factors D and D_P are closely related for the stagnant flow conditions considered in Refs. 1 and 2 where $\bar{u} = 0$, noting that the effect of the different powers of C_d in Eqs. (7) and (8) is small because C_d is on the order of unity for the conditions of all of these experiments (see Table 1). Based on the measurements of Refs. 1 and 2, this correspondence between the two correlations suggests that $n = \frac{3}{2}$. This estimate is reasonably close to the value $n = \frac{5}{4}$ suggested by Batchelor and Townsend,[11,12] where Eq. (4) is used to correlate turbulence intensities in the final-decay period of grid-generated turbulence, which is also consistent with the present relatively small values of Re_λ noted earlier.

Present measurements of streamwise and cross-stream relative turbulence intensities, within the turbulent interwake region for all three particle sizes, are plotted in Fig. 1 as a function of D according to Eq. (6). The correlation is seen to be remarkably good, over the two-order-of-magnitude range of D considered during the present experiments. Best-fit correlations of the measurements found by linear regression had powers of 0.48 and 0.56 (with standard deviations of both these powers of 0.03) for streamwise and cross-stream relative turbulence intensities, respectively. As a result, there is no statistical significance for the differences between the powers of these fits and the value of $n = \frac{3}{2}$ found in Refs. 1 and 2. Thus, for consistency with this earlier work, the measurements were correlated as shown in Fig. 1 using the earlier value of n to yield

$$\bar{u}'/U_p = 9.2 D^{\frac{1}{2}}, \qquad \bar{v}'/U_p = 7.9 D^{\frac{1}{2}} \qquad (9)$$

The standard deviation of the coefficients of Eqs. (9) are 1.5 and 1.6, respectively, and the correlation coefficients of both these fits are 0.98, which is excellent.

The difference between the coefficients of the streamwise and the cross-stream relative turbulence intensities is not statistically significant. Thus, the turbulent interwake region is isotropic within present capabilities to evaluate this behavior. Slight anisotropy favoring the streamwise direction, however, is not unexpected. In particular, the present wake discrimination system was not totally effective as discussed later, which introduces some streamwise velocity bias because of uneliminated streamwise mean velocity disturbances from wakes. In addition, past studies of grid-generated turbulence at small turbulence Reynolds numbers [Re_λ of 36–72, which is somewhat larger than the present range (see Table 1)] from Bennett and Corrsin[16] yielded values of $\bar{u}'/\bar{v}'$ in the range 1.09–1.22, which is similar to the present mean value of $\bar{u}'/\bar{v}' = 1.16$ found from Eqs. (9). Thus, potential for a small fundamental level of anisotropy for the turbulent interwake region cannot be ruled out.

The correspondence between the correlations of Eq. (6) involving D, based on sole consideration of the turbulent interwake region, and involving D_P, based on sole consideration of wake disturbances, helps explain the effectiveness of D_P for consideration the relative turbulence intensities observed in Refs. 1 and 2, even though the
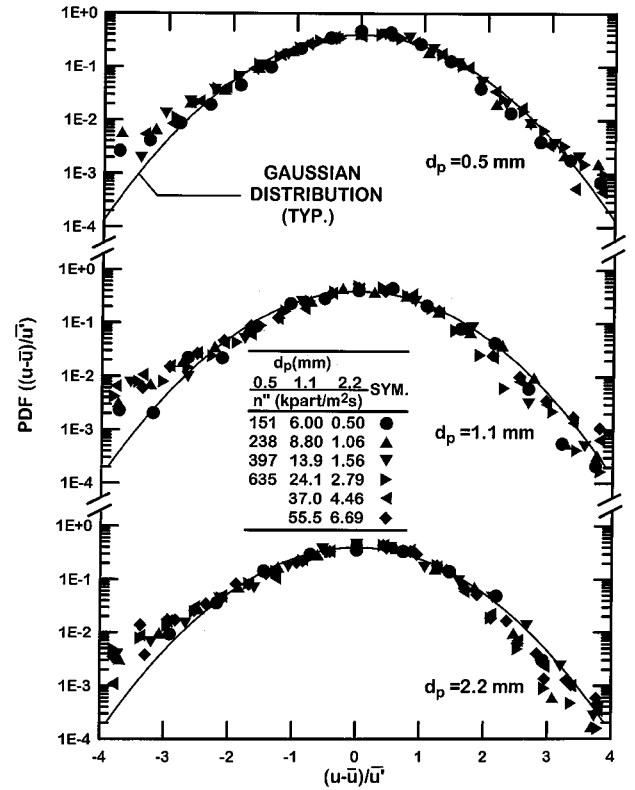

Fig. 2 Typical PDFs of streamwise velocities for various particle sizes and number fluxes.

wake disturbances did not contribute significantly to these measurements (i.e., wake disturbances were largely eliminated by their phase-discrimination systems). Thus, the nearly identical definitions of D and D_P suggest that either approach is fortuitously appropriate for both the turbulent interwake and wake disturbance regions of flows caused by turbulence generation (even though the detailed properties of these two flow regions differ considerably).

PDFs

Potential departures of the turbulent interwake region from the behavior of isotropic turbulence were studied further by considering the PDFs and the higher-order (skewness and kurtosis) statistical moments of streamwise and cross-stream velocities. Typical measured streamwise and cross-stream PDFs of velocities for various particle sizes and loadings are plotted in Figs. 2 and 3. Fits of the measurements are also shown on the plots, corresponding to best Gaussian fits based on rms velocity fluctuations. These PDFs are plotted using logarithmic scales to highlight potential effects of wake disturbances and the performance of the fits at the extremities of the distributions where the PDFs become small.

PDFs of cross-stream velocities illustrated in Fig. 3 are symmetric, which is consistent with absence of any preferred direction for cross-stream velocities because of contributions from either the turbulent interwake region or from wake disturbances that were not completely eliminated by the wake discrimination system of the LV. The cross-stream PDFs are also in generally good agreement with the Gaussian fits. The main exceptions are slight upward biases near both edges of the distributions, which are thought to be caused by increased experimental uncertainties near the extremities of the distributions because of sampling limitations (e.g., normalized PDFs at these locations are very small, on the order of 10^{-3}).

In contrast to the symmetric PDFs of cross-stream velocities, the PDFs of streamwise velocities illustrated in Fig. 2 exhibit a distinct asymmetry. This involves an upward bias of the measurements from the Gaussian distribution near -2.5 standard deviations, whereas the positive sides of the distributions agree quite well with Gaussian distributions. This behavior, however, no doubt results from small disturbances caused by mean streamwise velocities in the particle wakes that were not eliminated by the present particle wake discrimination system.
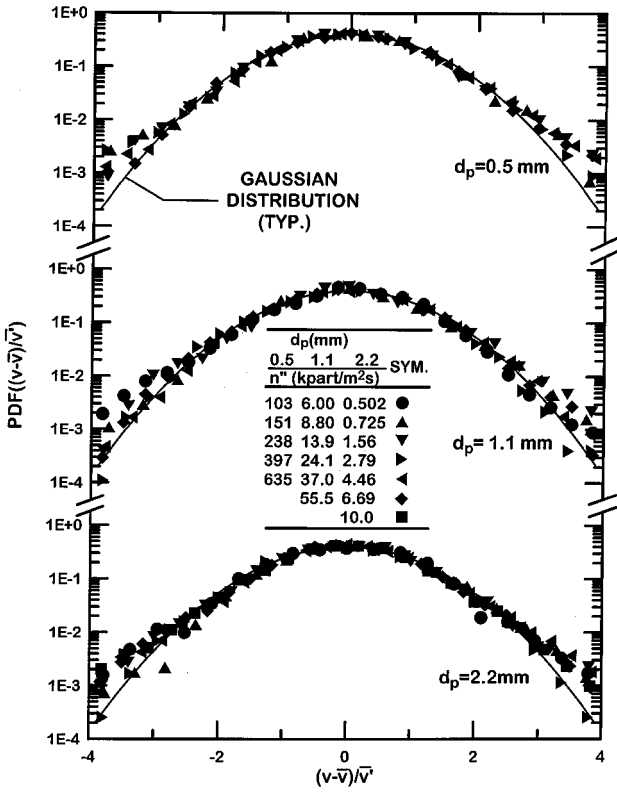
Fig. 3   Typical PDFs of cross-stream velocities for various particle sizes and number fluxes.

Fig. 4   Energy spectra of streamwise velocity fluctuations for various particle sizes and number fluxes.

Higher moments of the PDFs averaged over all of the measurements in the turbulent interwake region, can be summarized as follows: values of $S(u)$ and $S(v)$ are -0.5 and 0.0, with standard deviations of 0.4 and 0.1, respectively; and values of $K(u)$ and $K(v)$ are 7 and 8, both with standard deviations of 2. The departures of measured values of skewness from the Gaussian value of $S = 0$ are not statistically significant, although the measurements do suggest a contribution of wake disturbances to the somewhat larger negative skewness of the PDF of streamwise velocities. The departures of the measured values of kurtosis from the Gaussian value of $K = 3$ also borders on the limit of statistical significance, particularly in view of the larger experimental uncertainties of this high-order moment caused by sampling limitations. Thus, the present PDF measurements within the turbulent interwake region are adequately described by Gaussian functions, similar to conventional isotropic turbulence.

Energy Spectra

Streamwise energy spectra within the turbulent interwake region were obtained using Taylor's hypothesis to transform measured temporal spectra to spatial spectra as already described. The corresponding integral length scales were found by noting that the normalized amplitude of the energy spectra plots $2\pi E_u(k)/(\bar{u}'^2 L_u)$ approaches the value of four as the normalized wave number of these plots $kL_u/(2\pi)$ becomes small, analogous to temporal spectra as discussed by Hinze.[10] The resulting normalized energy spectra of streamwise velocity fluctuations are illustrated in Fig. 4 for various particle sizes and loadings. Correlations of energy spectra for approximate isotropic turbulence are also shown on the plot for comparison with the measurements. The approximate spectra represent the simplification of isotropic turbulence discussed by Hinze,[10] where correlations of velocity fluctuations are assumed to satisfy exponential functions. This simplification implies that the $-\frac{5}{3}$ power decay of the energy spectra within the inertial subrange of turbulence is approximated by a -2 power decay.

Although the energy spectra illustrated in Fig. 4 are separated by particle sizes to help readability, the spectra are independent of both particle size and loading and agree reasonably well with the isotropic turbulence approximation described by Hinze.[10] Thus, the prominent -1 power decay region of the spectra of the over-
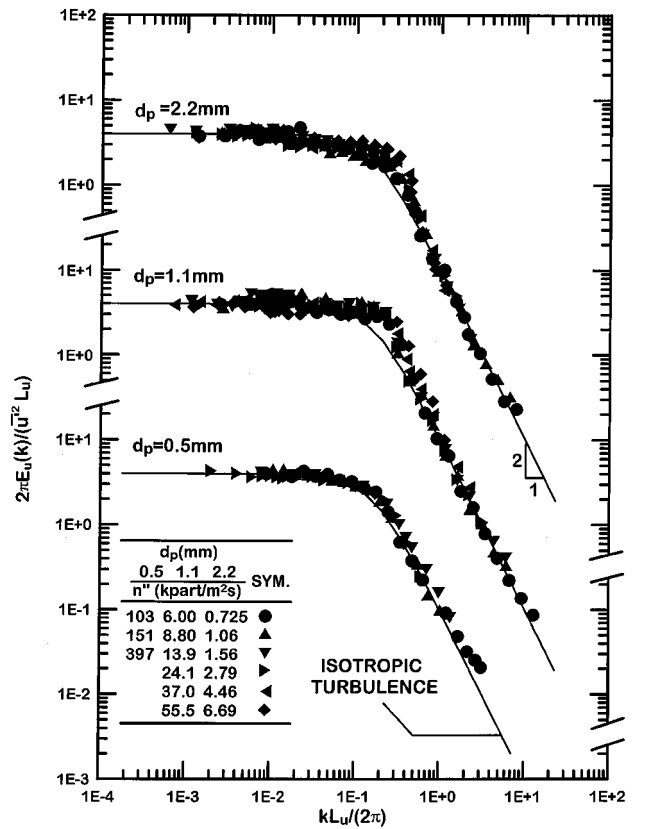
all flow (wake disturbances plus the turbulent interwake region) of continuous-phase turbulence resulting from turbulence generation, seen in Refs. 1–3, disappears when the particle wake disturbances are removed. This finding implies that the -1 power decay region seen for the overall flow is caused by wake disturbances. Finally, the present spectra are truncated at large wave numbers to avoid step noise caused by sampling limitations, with full spectra expected to reach wave numbers characteristic of Kolmogorov scales at values of $kL_u/(2\pi)$ on the order of 100. Thus, the present interwake turbulence exhibits a substantial range of scales, roughly 1000:1, even though turbulence Reynolds numbers are small, less than 4. Consideration of length scales in the present turbulent interwake regions, however, will show that the present large range of scales represent reasonable behavior for turbulence in the final decay period, which is characteristic of the turbulent interwake region for present test conditions. These same considerations of length scales will also show that the present large range of scales appears for very different reasons than in high-Reynolds-number isotropic turbulence. This behavior will be discussed next.

Length Scales

Numerous studies of isotropic turbulence at large turbulence Reynolds numbers show that the rate of dissipation of turbulence kinetic energy can be estimated from values of velocity fluctuations and integral length scales using the following equation[10]:

$$A = \varepsilon L_u / (\bar{u}')^3 \qquad (10)$$

where A, the dimensionless integral length scale, is believed to be a constant on the order of unity. All properties on the right-hand side of Eq. (10) have been measured during the present investigation so that values of A can be found at much smaller Re_λ than considered in the past.

The resulting values of A from the present investigation are plotted as a function of Re_λ in Fig. 5, providing results at small Reynolds numbers $Re_\lambda = 0.4$–3.5. Results for isotropic turbulence from several past experiments,[17–21] from direct numerical simulations (DNS),[22–25] and from a DNS data fit from Sreenivasan[26] are plotted along with the present measurements. The earlier
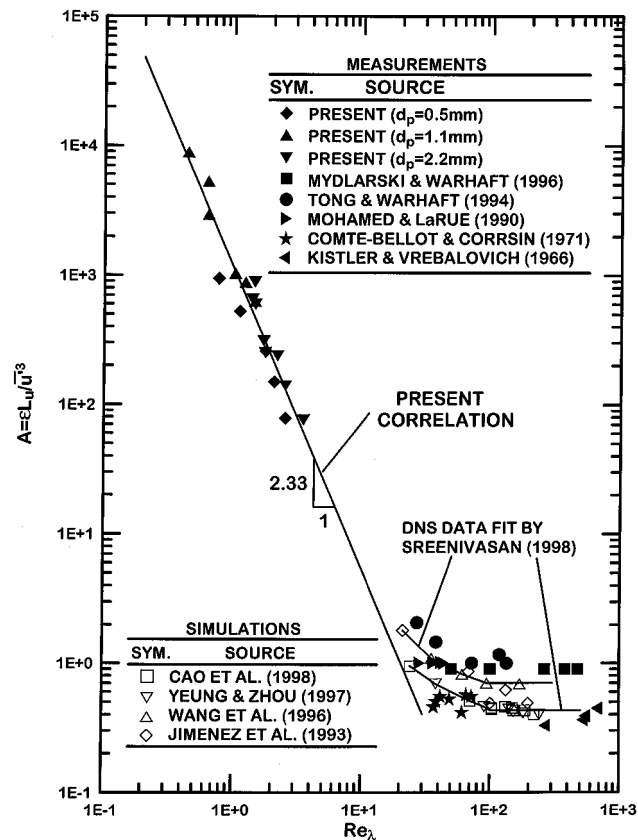
Fig. 5 Normalized integral length scales as a function of turbulence Reynolds number for both grid-generated and particle-generated turbulence. Measurements of Kistler and Vrebalovich,[17] Comte-Bellot and Corrsin,[18] Mohamed and LaRue,[19] Tong and Warhaft,[20] Mydlarski and Warhaft,[21] and the present investigation; predictions of Jiminez et al.,[22] Wang et al.,[23] Yeung and Zhou,[24] and Cao et al.[25]; DNS data fit of Sreenivasan.[26]

determinations of A involve relatively large turbulence Reynolds numbers, $20 \le Re_\lambda \le 800$, which places these flows in the initial decay period of isotropic turbulence where the turbulence is fully developed and acts over the entire flow region similar to conventional turbulence. In contrast, present measurements at small values of Re_λ exhibit very enhanced rates of dissipation, which is typical of behavior in the final-decay period where the vorticity is sparse and turbulence appears to involve disconnected spots when single-point measurements are observed.[4,11,12,27,28] This behavior is also consistent with earlier indications that interwake turbulence was in the final-decay period, based on relative turbulence intensities as discussed in connection with Fig. 1.

The measurement and predictions at large Re_λ yield scattered values of A in the range 0.3–2.0, which is on the order of unity and independent of Re_λ, as expected. Sreenivasan[26] suggests that these variations of A are caused by different initial conditions or grid geometries of the flows that were considered. In contrast, present values within the final-decay period indicate strongly enhanced dissipation as Re_λ decreases (indicated by increasing values of A), analogous to strongly enhanced dissipation as Re_λ decreases (indicated by decreasing values of the turbulence intensity) along the axis of turbulent wakes in the final-decay period (see Ref. 4). The present measurements of A within the final-decay period yield a best fit correlation as follows:

$$A = 1130 Re_\lambda^{-2.33}, \qquad 0.4 \le Re_\lambda \le 3.5 \qquad (11)$$

where the experimental uncertainty of the power of Re_λ is 0.16 and the correlation coefficient of the fit is 0.96. Combining all of the observations of A illustrated in Fig. 5, it is evident that A exhibits three regimes: 1) a large Re_λ regime (the initial-decay period) with $Re_\lambda > 100$, which corresponds to classical homogeneous isotropic turbulence at large Reynolds numbers; 2) a small Re_λ regime (the

final-decay period) where $Re_\lambda < 10$, which corresponds to present turbulent interwake conditions; and 3) a transition regime with $10 < Re_\lambda < 100$ between the two outer limiting regimes.

It is interesting to consider the variation of the length scale ratio L_u/λ as a function of Re_λ, in the three regimes of A that were just defined. This ratio assumes the following forms.

Final-decay period:

$$L_u/\lambda = 75 Re_\lambda^{-1.33}, \qquad 0.4 \le Re_\lambda \le 3.5 \qquad (12)$$

Initial-decay period:

$$L_u/\lambda = A Re_\lambda/15, \qquad 20 \le Re_\lambda \qquad (13)$$

Finally, in the transition region, Ling and Huang[27] find $A \sim Re_\lambda^{-1}$, which implies the following.

Transition period:

$$L_u/\lambda = 2.2, \qquad 4 \le Re_\lambda \le 20 \qquad (14)$$

The correlations of Eqs. (12–14) are illustrated in Fig. 6, along with results from available measurements and DNS simulations. Taken together, the various correlations provide reasonably good fits of results in the final-decay, transition, and initial-decay periods.

The nature and location of transition to the final-decay period seen in Fig. 6 seems quite reasonable. In particular, the variation of L_u/λ with decreasing Re_λ for fully developed turbulent flows must change as Re_λ becomes small because realizable flow properties cannot involve a Taylor length scale (a microscale) larger than the integral scale (a macroscale), or conditions where $L_u/\lambda < 1$. Thus, it is not surprising that the transition to the final-decay period, where L_u/λ increases with decreasing Re_λ, occurs when L_u/λ reaches values on the order of unity.

Increasing values of L_u/λ with increasing Re_λ in the initial-decay period is well understood[8,10] as a result of the relatively inviscid large-scale features (on the scale of integral scales) combined
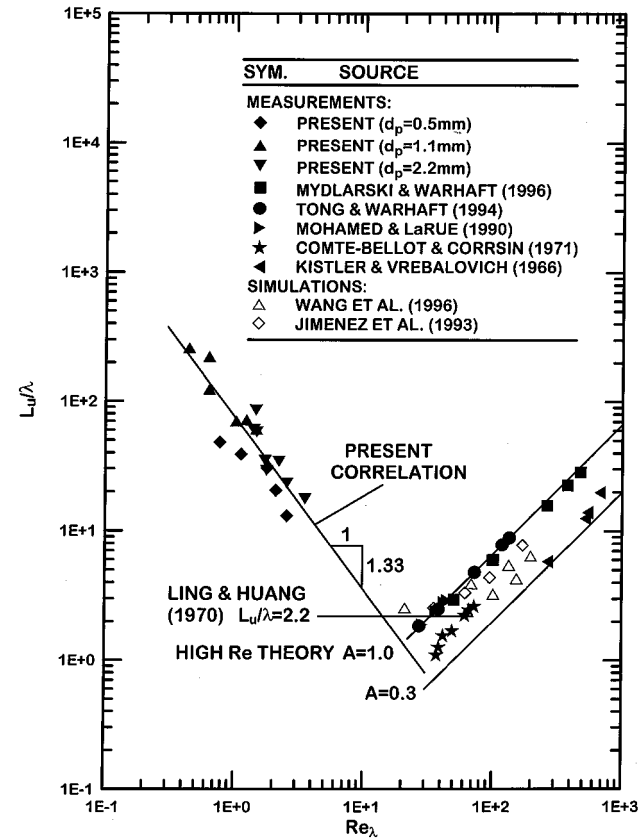

Fig. 6 Ratios of integral and Taylor length scales as a function of turbulence Reynolds number for both grid-generated and particle-generated turbulence. Measurements of Kistler and Vrebalovich,[17] Comte-Bellot and Corrsin,[18] Mohamed and LaRue,[19] Tong and Warhaft,[20] Mydlarski and Warhaft,[21] and the present investigation; predictions of Jiminez et al.[22] and Wang et al.[23]; correlation of Ling and Huang.[27]

with progressively smaller microscales of turbulence as turbulence Reynolds numbers increase. The corresponding increasing values of L_u/λ with decreasing values of Re_λ in the final-decay period occurs for very different reasons. In this case vortical regions are sparse although they still spread throughout the entire flow, yielding large integral scales in the presence of small dissipation scales, i.e., the dimensions of turbulent spots become small in comparison to the dimensions of the flow as a whole when the vortical regions of the flow become more sparse as turbulence decay proceeds.

Conclusions

This investigation considered the properties of turbulence generated by uniform fluxes of monodisperse spherical particles moving through air at standard temperature and pressure, emphasizing the properties of the turbulent interwake region. Test conditions included nearly monodisperse glass beads having diameters of 0.5–2.2 mm, particle Reynolds numbers of 106–990, mean particle spacings of 13–208 mm, particle volume fractions less than 0.003%, direct rates of dissipation of turbulence by particles less than 4%, and turbulence generation rates sufficient to yield streamwise relative turbulence intensities of 0.2–1.5%. The major conclusions of the study are as follows:

1) The turbulent interwake region is homogeneous and nearly isotropic with PDFs of streamwise and cross-stream velocities well approximated by Gaussian functions.

2) Relative turbulence intensities in the turbulent interwake region were correlated effectively by analogy to the known properties of isotropic grid-generated turbulence, e.g., Batchelor and Townsend,[11,12] by scaling these properties with the mean particle spacing normalized by the particle wake momentum diameter to yield a dimensionless dissipation factor.

3) The present dimensionless dissipation factor, based on consideration of interwake turbulence alone, is nearly identical to an earlier dimensionless dissipation factor found in Refs. 1 and 2, based on consideration of particle wake properties alone. This fortuitous agreement of correlations for the turbulent interwake region and for wake disturbances is no doubt responsible for the simple correlations of overall relative turbulence intensities (involving both regions) as a function of dimensionless dissipation factor observed during earlier work.[1–3]

4) For present turbulence generation conditions and probably for most practical dispersed flows, the turbulent interwake region exhibited very small turbulence Reynolds numbers ($Re_\lambda < 4$) and was in the final-decay period where vortical regions fill the entire interwake region but are sparse, i.e., where turbulence appears to involve disconnected turbulent spots when single-point measurements are observed.

5) Within the final-decay period macroscale/microscale ratios (e.g., L_u/λ) decrease with increasing turbulence Reynolds numbers as opposed to increasing similar to fully developed isotropic turbulence at large turbulence Reynolds numbers. Quite plausibly, the transition from the final-decay region to the fully developed turbulence region occurs when L_u/λ is on the order of unity; this condition corresponds to a turbulence Reynolds number on the order of 10, which is similar to conditions at the transition of turbulent wakes in nonturbulent environments to the final decay period (see Ref. 4).

Acknowledgments

References

[1]Parthasarathy, R. N., and Faeth, G. M., "Turbulence Modulation in Homogeneous Dilute Particle-Laden Flows," *Journal of Fluid Mechanics*, Vol. 220, Pt. 2, 1990, pp. 485–514.

[2]Mizukami, M., Parthasarathy, R. N., and Faeth, G. M., "Particle-Generated Turbulence in Homogeneous Dilute Dispersed Flows," *International Journal of Multiphase Flow*, Vol. 18, No. 2, 1992, pp. 397–412.

[3]Chen, J.-H., Wu, J.-S., and Faeth, G. M., "Turbulence Generation in Homogeneous Particle-Laden Flows," *AIAA Journal*, Vol. 38, No. 4, 2000, pp. 636–642.

[4]Wu, J.-S., and Faeth, G. M., "Sphere Wakes in Still Surroundings at Intermediate Reynolds Numbers," *AIAA Journal*, Vol. 31, No. 8, 1993, pp. 1448–1455.

[5]Wu, J.-S., and Faeth, G. M., "Sphere Wakes at Moderate Reynolds Numbers in a Turbulent Environment," *AIAA Journal*, Vol. 32, No. 3, 1994, pp. 535–541.

[6]Wu, J.-S., and Faeth, G. M., "Effects of Ambient Turbulence Intensity on Sphere Wakes at Intermediate Reynolds Numbers," *AIAA Journal*, Vol. 33, No. 1, 1995, pp. 171–173.

[7]Chen, J.-H., "Turbulence Generation in Homogeneous Dilute Particle-Laden Flows," Ph.D. Dissertation, Dept. of Naval Architecture and Marine Engineering, Univ. of Michigan, Ann Arbor, MI, 1999.

[8]Schlichting, H., *Boundary Layer Theory*, 7th ed., McGraw–Hill, New York, 1979, pp. 234, 235, 599.

[9]Tennekes, H., and Lumley, J. L., *A First Course in Turbulence*, MIT Press, Cambridge, MA, 1972, pp. 113–124, 196–201.

[10]Hinze, J. O., *Turbulence*, 2nd ed., McGraw–Hill, New York, 1975, Chap. 3, pp. 65–67, 204, 496–519.

[11]Batchelor, G. K., and Townsend, A. A., "Decay of Isotropic Turbulence in the Initial Period," *Proceedings of the Royal Society of London*, Vol. A193A, No. 8, 1948, pp. 539–558.

[12]Batchelor, G. K., and Townsend, A. A., "Decay of Turbulence in the Final Period," *Proceedings of the Royal Society of London*, Vol. 194A, No. 8, 1948, pp. 527–543.

[13]Buchhave, P., "The Measurement of Turbulence with the Burst-Type Laser Doppler Anemometer—Errors and Correction Methods," Ph.D. Dissertation, Dept. of Mechanical and Aerospace Engineering, State Univ. of New York, Buffalo, NY, 1979.

[14]Buchhave, P., George, W. K., and Lumley, J. L., "The Measurement of Turbulence with the Laser-Doppler Anemometer," *Annual Review of Fluid Mechanics*, Vol. 11, 1979, pp. 443–504.

[15]Rice, S. O., "Mathematical Analysis of Random Noise," *Noise and Stochastic Processes*, edited by N. Wax, Dover, New York, 1954, pp. 133–294.

[16]Bennett, J. C., and Corrsin, S., "Small Reynolds Number Nearly Isotropic Turbulence in a Straight Duct and a Contraction," *Physics of Fluids*, Vol. 21, No. 12, 1978, pp. 2129–2140.

[17]Kistler, A. L., and Vrebalovich, T., "Grid Turbulence at Large Reynolds Numbers," *Journal of Fluid Mechanics*, Vol. 26, Pt. 1, 1966, pp. 37–47.

[18]Comte-Bellot, G., and Corrsin, S., "Simple Eulerian Time Correlation of Full- and Narrow-Band Velocity Signals in 'Grid-Generated', Isotropic Turbulence," *Journal of Fluid Mechanics*, Vol. 48, Pt. 2, 1971, pp. 273–337.

[19]Mohamed, M. S., and La Rue, J. C., "The Decay Power Law in Grid-Generated Turbulence," *Journal of Fluid Mechanics*, Vol. 219, Pt. 1, 1990, pp. 195–214.

[20]Tong, C., and Warhaft, Z., "On Passive Scalar Derivative Statistics in Grid Turbulence," *Physics of Fluids*, Vol. 6, No. 6, 1994, pp. 2165–2176.

[21]Mydlarski, L., and Warhaft, Z., "On the Onset of High-Reynolds-Number Grid-Generated Wind Tunnel Turbulence," *Journal of Fluid Mechanics*, Vol. 320, Pt. 2, 1996, pp. 331–368.

[22]Jiminez, J., Wray, A. A., Saffman, P. G., and Rogallo, R. S., "The Structure of Intense Vorticity in Isotropic Turbulence," *Journal of Fluid Mechanics*, Vol. 255, Pt. 1, 1993, pp. 65–90.

[23]Wang, L.-P., Chen, S., Brasseur, J. G., and Wyngaard, J. C., "Examination of Hypotheses in the Kolmogorov Refined Turbulence Theory Through High-Resolution Simulations, Part I Velocity Field," *Journal of Fluid Mechanics*, Vol. 309, Feb. 1996, pp. 113–156.

[24]Yeung, P. K., and Zhou, Y., "On the Universality of the Kolmogorov Constant in Numerical Simulation of Turbulence," *Physical Review E*, Vol. 18, No. 7, 1997, p. 1746.

[25]Cao, N., Chen, S., and Doolen, G. D., "Statistics and Structure of Pressure in Isotropic Turbulence," cited by Sreenivasan.[26]

[26]Sreenivasan, K. R., "An Update on the Energy Dissipation Rate in Isotropic Turbulence," *Physics of Fluids*, Vol. 10, No. 2, 1998, p. 529.

[27]Ling, S. C., and Huang, T. T., "Decay of Weak Turbulence," *Physics of Fluids*, Vol. 13, No. 12, 1970, pp. 2912–2924.

[28]Phillips, O. M., "The Final Period of Decay of Non-Homogeneous Turbulence," *Proceedings of the Cambridge Philosophical Society*, Vol. 52, Pt. 1, 1956, pp. 135–151.

R. M. C. So
Associate Editor